An Examination of the Effect of Boundary Layer Ingestion on Turboelectric Distributed Propulsion Systems

James L. Felder[1], Hyun Dae Kim[2], and Gerald V. Brown[3]
NASA Glenn Research Center, Cleveland, OH, 44135, USA

and

Julio Chu[5]
NASA Langley Research Center, Hampton, VA, 23681-2199, USA

A Turboelectric Distributed Propulsion (TeDP) system differs from other propulsion systems by the use of electrical power to transmit power from the turbine to the fan. Electrical power can be efficiently transmitted over longer distances and with complex topologies. Also the use of power inverters allows the generator and motors speeds to be independent of one another. This decoupling allows the aircraft designer to place the core engines and the fans in locations most advantageous for each. The result can be very different installation environments for the different devices. Thus the installation effects on this system can be quite different than conventional turbofans where the fan and core both see the same installed environments. This paper examines a propulsion system consisting of two superconducting generators, each driven by a turboshaft engine located so that their inlets ingest freestream air, superconducting electrical transmission lines, and an array of superconducting motor driven fan positioned across the upper/rear fuselage area of a hybrid wing body aircraft in a continuous nacelle that ingests all of the upper fuselage boundary layer. The effect of ingesting the boundary layer on the design of the system with a range of design pressure ratios is examined. Also the impact of ingesting the boundary layer on off-design performance is examined. The results show that when examining different design fan pressure ratios it is important to recalculate of the boundary layer mass-average Pt and MN up the height for each inlet height during convergence of the design point for each fan design pressure ratio examined. Correct estimation of off-design performance is dependent on the height of the column of air measured from the aircraft surface immediately prior to any external diffusion that will flow through the fan propulsors. The mass-averaged Pt and MN calculated for this column of air determine the Pt and MN seen by the propulsor inlet. Since the height of this column will change as the amount of air passing through the fans change as the propulsion system is throttled, and since the mass-average Pt and MN varies by height, this "capture height" must be recalculated as the airflow through the propulsor is varied as the off-design performance point is converged.

Nomenclature

ADP = Aerodynamic Design Point
BSCCO = bismuth strontium calcium copper oxide

[1] Aerospace Engineer, Systems Engineering and Analysis Division, 21000 Brookpark Rd/MS 86-4, Senior Member.
[2] Aerospace Engineer, Aeropropulsion Division, 21000 Brookpark Road, MS 5-11, Senior Member.
[3] Senior Research Engineer, Structures and Materials Division, 21000 Brookpark Road, MS 49-8.
[4] Aerospace Engineer, Aeronautics Systems Analysis Branch, MS 442

CMC = Ceramic Matrix Composite
Fn = Net thrust
HWB = Hybrid Wing Body Aircraft
MgB2 = Magnesium DiBoride
MN = Mach number
MN_{avg} = Mass-averaged Mach number of the boundary-layer to a given height
NPSS = Numerical Propulsion System Simulation
PR = Pressure Ratio
Pt_{avg} = Mass-averaged total pressure of the boundary-layer to a given height
RTO = Rolling Take-Off – Sea Level, Mach 0.25, ISA+27R
TeDP = Turboelectric Distributed Propulsion
TSFC = Thrust Specific Fuel Consumption

I. Introduction

THE NASA Subsonic Fixed Wing (SFW) project has defined ambitious goals for the next three generations of aviation (termed N+1, N+2, N+3)[1]. To meet the N+3 goals for fuel burn, noise, emissions and field length reduction will take innovative approaches to aircraft and propulsion technology and design. One approach being examined by a team at the NASA Glenn and Langley Research Centers is the combination of a hybrid wing body aircraft being driven by a distributed propulsion system that transmits power from the turbine to the fan electrically rather than mechanically. This paper reports the results of an examination into the impact of ingesting the boundary layer on the design of a Turboelectric Distributed Propulsion (TeDP) system integrated into hybrid wing body (HWB) aircraft we labeled the N3-X. The TeDP system and the N3-X aircraft are expansion of and correction to results originally presented at the 2009 AIAA Aerospace Science Meeting[2].

The TeDP system consists of two turboshaft engines driving superconducting generators that produce electricity that is then used to power an array of superconducting electric motor driven propulsors. The turbogenerators are located on the wingtips and therefore have freestream inlet conditions. The propulsors are located in a continuous array that spans the entire upper rear fuselage section so as to capture the entire boundary layer from the top of the fuselage section. The number of propulsors in the array is allowed to vary with the design FPR. A TeDP thermodynamic cycle simulation model was constructed in the Numerical Propulsion System Simulation (NPSS)[3,4] program utilizing current estimates of turbine engine component technologies and efficiency anticipated to be available in the N+3 timeframe. The N3-X aircraft system is a merger of the concept aircraft from the 2009 ASM paper with additional HWB development work ongoing at Langley which in turn is an expansion on the N2A hybrid wing body (HWB) aircraft[5] .

Figure 1. N3-X with Turboelectric Distributed Propulsion System

The propulsors are deliberately positioned to ingest the boundary layer. The diffusion or inlet drag of a propulsion system is the force required to decelerate the incoming air and is thus proportional to the velocity of the incoming air. Ingesting the boundary layer allows the propulsion system to take advantage of the deceleration of the aircraft boundary layer due to viscous forces to reduce the inlet velocity of the propulsor and thus reduce the amount of inlet drag. If the fan nozzle is unchoked, the slower inlet velocity also results in a slower exit velocity. As described by Plas[8] for systems that ingest the boundary layer, the propulsive efficiency is given by

$$\eta_p = \frac{2U_0}{\left(U_j + U_{in}\right)} \tag{1}$$

Where U_o is the freestream velocity, U_{in} is the inlet velocity, and U_j is the nozzle exit velocity. If $U_{in} = U_o$, then Eq. (1) simplifies to the standard form of the equation for propulsive efficiency.

$$\eta_p = \frac{2}{\left(1 + \frac{U_j}{U_0}\right)} \tag{2}$$

II Simulation Configuration, Inputs and Assumptions

The following are the inputs and design assumption made to construct the TeDP system simulation model in NPSS

A. Aircraft Thrust Requirements

The N3-X aircraft is designed to carry an 118,100 lbm payload 7500 nm at Mach 0.84. These mission requirements yield the following thrust requirements. The TeDP system was sized at the aerodynamic design point (ADP). Thrust was checked against the minimum thrust for the sea level, MN 0.25, ISA+27R day rolling take-off (RTO) and sea level, static, ISA day take-off (T/O). The design thrust at the ADP is adjusted if necessary to provide the minimum thrust levels at the other two key flight conditions.

Table 1. N3-X Thrust Requirements

Flight Condition	Minimum Thrust Required
Aerodynamic Design Point (ADP) (30,000 ft / MN 0.84 / ISA)	26,750 lbf
Rolling Take-Off (RTO) (SL / MN 0.25 / ISA+27 R)	65,000 lbf
Sea Level Static Take-off (T/O) (SL / MN 0.0 / ISA)	90,000 lbf

B. Propulsor Array

The motor driven propulsors are assumed to be positioned in a continuous array across the upper rear surface of the fuselage section with the inlet as close to the trailing edge as possible. The propulsor array forms a wide V shape with the bottom of the V at the center line and the arms moving forward to follow the trailing edge. The inlets and nozzles for this array of propulsors form a continuous 2-D slot with internal vertical dividers separating the flow to each individual propulsor. The maximum span-wise distance available on the after upper fuselage section is set at 60 feet. This span is assumed to always be filled by the propulsor array, thus the width of the inlet to each propulsor is determined by the number of propulsors in the array. As the total airflow required changes due to changes in the fan pressure ratio, only the height of the propulsor array changes to yield the required changes in the inlet and nozzle areas.

The number of propulsors is assumed to always be an odd number. This means that there is always a single centerline propulsor with an equal number of propulsors on either side. The reason for this restriction is so that in a V-shape of the propulsor array no fan rotor is coplanar with the fan rotor on either side. We assume that with sufficient containment ring thickness that the relatively small low energy fan blades could be contained in the event of a blade failure. Thus penetration into the neighboring propulsors should not be an issue. The axial off-set should prevent distortion in the walls of a propulsor cell due to failure of a fan in a neighboring propulsor from causing a cascade of fan failures.

1. Inlet Conditions

A 3-D CFD simulation of the top surfaces of the related N2A-EXTE was conducted by Boeing[9]. The Mach contours of the inviscid flow at the top of the boundary layer from this simulation are presented in Fig. 2. This simulation yielded velocity, temperature and pressure profiles as a function of the distance above the fuselage ranging from the aircraft surface to undisturbed air several thousand inches above the aircraft. Most of the data points, however, were concentrated in the boundary layer. Profiles along the centerline from 60% to 100% of the fuselage chord length are shown in Fig. 3. Compared to the N3-X aircraft, the N2A-EXTE aircraft has an extended center

fuselage section. The result is that N2A-EXTE has a fuselage length of 1,800 inches, while the N3-X has a fuselage length of 1600 inches. Despite this difference in absolute length, it was judged that the boundary layer profile shapes at the same percent chord length would be very similar between the two aircraft. When determining the percent chord location of the inlet for the propulsor array, the shorter 1,600 inch fuselage length was used.

A profile of the mass-average MN and Pt (MN_{avg}, Pt_{avg}) was calculated from the boundary layer profiles. The mass average MN and Pt for each distance "i" in the profile was calculated from the Eq. (3) and Eq. (4), where m_i is the mass flow through the i^{th} segment of the boundary layer, MN_i is the Mach number in the i^{th} segment, and Pt_i is the total pressure in the i^{th} segment

$$MN_{avg_i} = \sum_{0}^{i}(m_i MN_i) \Big/ \sum_{0}^{i} m_i \tag{3}$$

$$Pt_{avg_i} = \sum_{0}^{i}(m_i Pt_i) \Big/ \sum_{0}^{i} m_i \tag{4}$$

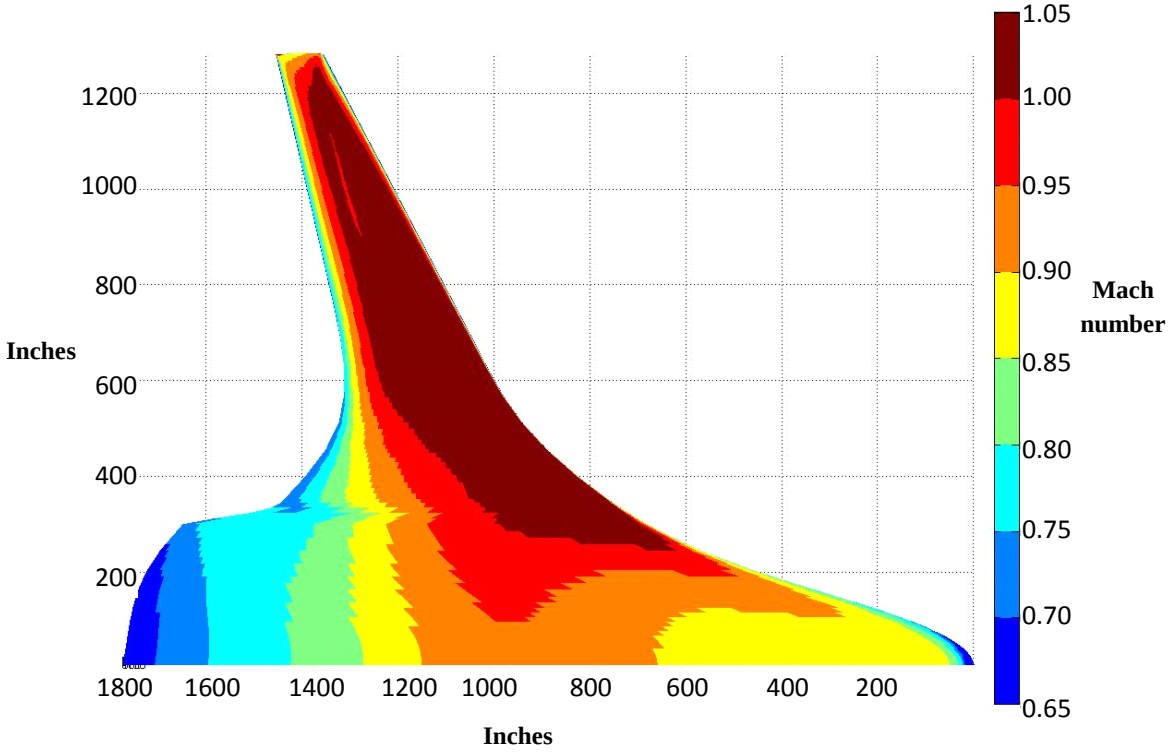

Figure 2. N2A-EXTE Mach Number Contours

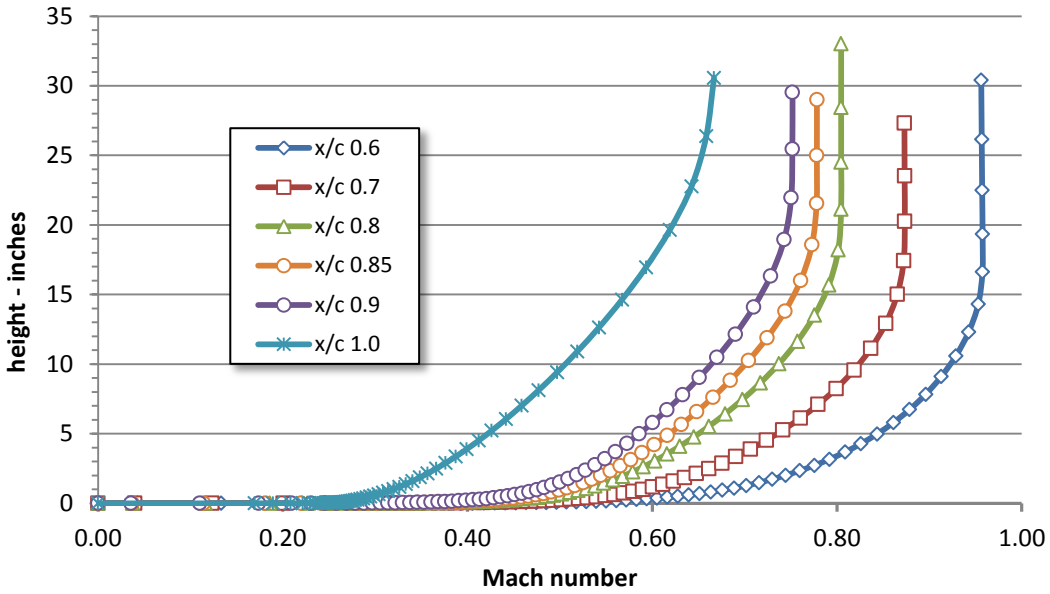

Figure 3. N2A-EXTE Centerline Mach Number Contours

The MN_{avg} and Pt_{avg} were divided by the freestream MN and Pt of 0.8 and 5.183 to yield normalized boundary shapes that could then be used at other similar flight conditions. A MN of 0.8 and at total pressure of 5.183 psia correspond to an altitude very close to 35,000 feet, thus these boundary layer profiles should be very representative of boundary layers for cruise altitudes and speeds of interest. Ideally the boundary layers would be generated for other flight conditions, especially those such as take-off and climb which are at considerably different speeds and altitudes. However, such data is not currently available, and so these normalized profiles were used for all flight conditions. This is certainly an area for future refinement. Figure 4 contains a plot of the PtRatio and MNratio normalized curves.

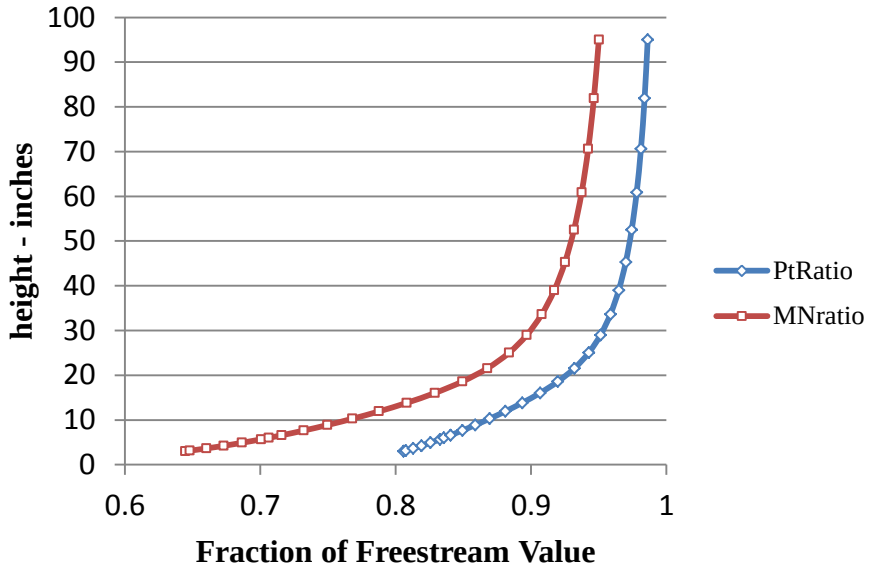

Figure 4. x/c = 0.85 Mass-avg PtRatio & MNratio

2. Inlet

The inlet for the propulsors is a continuous 2-D "mail-slot" inlet across the 60 foot span covered by the propulsor array. In order to have insight into the conditions at the physical inlet throat, the modeling of the inlet was divided into external and internal diffusion. This allows the inlet throat MN and static pressure to be calculated. However the critical parameter necessary to determine the inlet conditions is not the physical inlet height, rather it is the height of the capture sheet of air as measured at the point just before any external diffusion begins. When a range of different design fan pressure ratios were examined this capture height was varied so that it matched the inlet height on the assumption that the inlet height and capture height will be the same at the design point. During off-design analysis of a given design the capture height was varied such that the air flowing through a sheet of that height contains the mass flow required by the propulsors. It is the MN_{avg} and Pt_{avg} of this flow that determines the inlet drag of the propulsor. Any air above this height passes over the top of the propulsor nacelle. The result is that during off-design operation the incoming MN_{avg} and Pt_{avg} seen by the propulsor is throttle dependent.

3. Fan

Technology trend curves of fan efficiency and design tip speeds were developed by the Aerospace System Design Laboratory (ASDL) at Georgia Tech University for the FAA[10]. The trends were further updated as part of a NASA study examining advanced technology single-aisle transport to reflect the anticipated trends in 2015. These updated trends are presented in Fig. 5 and Fig. 6[11]. It was assumed that fan efficiency might advance an additional 0.5% to 1% in efficiency between 2015 and the N+3 technology readiness date of 2025.

However, an axial fan in an embedded installation will suffer a loss in efficiency due to pressure distortions resulting from ingesting the boundary layer. This loss was estimated by a recent NASA NRA study conducted by United Technologies Research Center (UTRC) and Pratt & Whitney to be about 2%, and perhaps as low as 1% with an inlet optimized to reduce distortion.[12] So for purposes of this study then a 1% penalty was assessed against the fan efficiencies given by Fig. 5 as an estimate of embedded fan technologies in the 2025 time frame. The design tip speeds given in Fig. 6 were used as given.

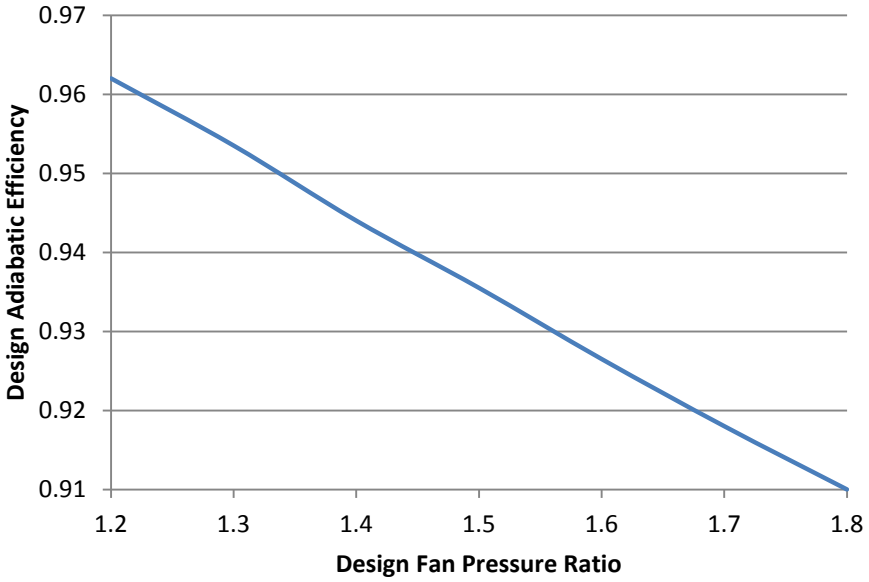

Figure 5. Fan design adiabatic efficiency as a function of design fan pressure ratio

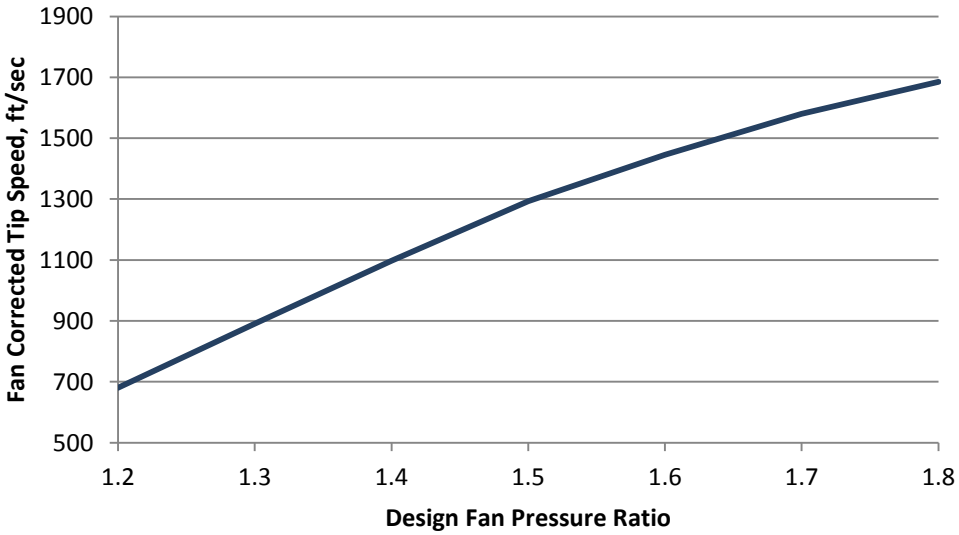

Figure 6. Fan Corrected Tip Speed as a function of design fan pressure ratio

4. Nozzle

The nozzle like the inlet is a continuous 2-D mail-slot design. Due to the low fan pressure ratio, the nozzle must have a variable exit area in order to keep the fan operation stable over a broad range of flight conditions. The 2-D geometry makes achieving a variable area fan nozzle much more straight forward than for the co-annular fan nozzle of a conventional turbofan engine.

5. Nacelle

The nacelle for the TeDP system is represented by the top and sides of the propulsor array. The only additional wetted area due to the nacelle compared to the wetted area of the bare aircraft fuselage covered by the propulsor array is the area of the sides of the propulsor array. The result is that with respect to the drag of the bare aircraft, we assume that the nacelle has no impact on drag. Thus the performance estimates here are for fully installed and not uninstalled performance. Further as the design FPR changes and the fan airflow changes as a result, the only change in the nacelle is to the areas of the size walls. This change in area is so minor that it was not included in this analysis. The effect of this attribute of a TeDP system is that the trend of rapidly growing external nacelle area with decreasing design FPR seen in pylon mounted engine system is not present with a TeDP system.

Table 2. Propulsor Design Parameters

Component/Attribute	Parameter	Design Value/Assumptions
Inlet	dP/P (throat to fan)	0.998
Fan	PR	1.30
	Adiabatic efficiency	0.9535
	Distortion efficiency penalty	0.01
	Design Tip Speed	883 ft/sec
Nozzle	Cdth	0.997
	Cv	0.997

C. Turbogenerators

The two turbogenerators are assumed to be mounted on the wing-tips. This is an unusual location for turbomachinery. However, in this application there are a number of advantages that accrue. One, as reinforced by the recent incident with the turbine rotor failure of the engine on the Qantas A380, is to minimize the risks to the aircraft, passengers and crew from high velocity debris in the event of a turbine disk failure. The wing-tip location means that there is a very narrow angle that any debris resulting from a turbine disk failure could impact the rest of the aircraft. Further the angle is narrow enough to entertain the idea of deflection of debris without prohibitive weight penalties. A multi-layered armored plate placed at an angle much like the front armor of military tanks could be situated at the wing tip just inboard of the turbogenerator to deflect any debris in the plane of the wing and avoid any further penetration. Other potential advantages include some span loading relief in the normal upward lift direction at the cost of designing for additional runway bump or gust loading, and an external mount that would facilitate maintenance and avoid thermal issues of a mount location buried inside the aircraft mold lines.

Each turbogenerator consists of a two spool gas generator feeding a power turbine which in turn drives a generator. The power turbine and generator are mounted on an independent third shaft. Whether this third shaft is coannular with the two gas generator shafts and the generator is mounted inside the inlet, or whether the generator is aft of the power turbine and the shaft is in-line with the gas generator shafts is not defined in this study, and will depend upon the heat leak rate through the generator case and the ability to route the turboshaft exhaust so as to avoid impinging on the generator.

The thermodynamic design point of the gas generator represents a very aggressive application of anticipated technology in the N+3 timeframe. The key turboshaft engine design parameters are listed in Table 3.

Table 3. Turbogenerator Design Parameters

Component/Attribute	Parameter	Design Value/Assumptions
Low pressure compressor (CompL)	Polytropic efficiency	0.9325
High pressure compressor (CompH)	Polytropic efficiency	0.9325
CompH	Maximum exit total temperature (T3)	1810 R @ RTO, 1681 R @ ADP
CompL & CompH	Pressure Ratio	Total PR varied to equal max T3 with an equal Δh split between compressors
Burner (Brn)	Exit total temperature (T4)	3460 R @ T/O, 3260 R @ ADP
High pressure turbine (TurbH)	Polytropic efficiency	0.93
Low pressure turbine (TurbL)	Polytropic efficiency	0.93
Power turbine (TurbP)	Polytropic efficiency	0.924
Turbine material	Ceramic Matrix Composite (CMC)	Uncooled for all hot section components including burner liner, and turbine stators and rotors
TurbH	Non-chargeable disk cooling	4%
TurbL	Non-chargeable disk cooling	2%
TurbP	chargeable disk cooling & cavity purge	1%
Nozzle	PRdes	2.0 @ 30k/MN0.84 ADP
	PRmin	1.08

D. Electrical System

The electrical system evaluated for this system consists of superconducting motors and generators with superconducting cables connecting them. Superconducting machines were examined due to their much higher power to weight ratio than the best ambient temperature machines. Also the overall efficiency of such devices as measured from shaft power into the generator to shaft power out of the motor exceeds 99%. The details of this system are explored in greater detail by Brown[13].

Key to the cycle modeling of the turboelectric system is that the generator power is rectified from AC to DC power, transmitted along DC power cables, and then converted back to AC by power inverters at each motor. The result is that there is no correlation between generator speed and fan motor speed. In effect the electrical power system in the TeDP system functions as an infinitely variable ratio gearbox

Further, within limits, the power and speed in a given generator or motor are also independent of each other. This allows the generator to operate at a power level and shaft speed that yields the best performance of the power turbine. The fan motor can also operate at the power level and shaft speed that yields the best fan performance. And since the speeds of the motors and generators are independent, both optimizations can be done at the same time.

For the analysis reported in this paper, these three degrees of freedom in design and operation were used to keep the Power Turbine operating at a constant corrected speed and the Fan operating on a line that follows the peak efficiency line.

1. Superconducting Materials

The superconducting portions of the system must be cooled to a temperature specific to the materials and design of the superconducting machine. Brown examined two different types of superconducting materials, bismuth strontium calcium copper oxide (BSCCO) and Magnesium DiBoride (MgB2). BSCCO is in the family of high temperature superconductors with critical temperatures around the boiling point of liquid nitrogen (77 K). The operating temperature is held to 50 K to allow for the high current densities necessary. The MgB2 material is a new class of superconductor discovered in 2001 that has a critical temperature intermediate between the very low (4 K) metallic superconductors and the high temperature (77K) class of superconductors represented by BSCCO. It has a transition temperature around 39 K, with operating temperatures no higher than 30 K.

2. Motors and Generators

The losses in the motors and generators were assumed to be the same. All losses for the current analysis are assumed to occur in the stator. The rotor operates with DC current and thus is subject only to resistive losses. Therefore, losses in the superconductor rotor approach zero.

3. Inverters

Each motor in the system has an inverter associated with it. While the temperature of the inverter does not have to be maintained at the same temperatures as the superconducting portions of the system, a recent design study shows that the losses and weight of the inverters are greatly reduced if the temperatures are held to 120 K or less[14]. In order to provide sufficient temperature difference for efficient heat transfer, a maximum of 100 K was used for inverter cooling calculations.

4. Cooling

Two different cooling methods were examined. One method used electrically driven cryocoolers to provide active refrigeration to pump the heat generated by losses in the superconducting machines and the inverters from the maximum allowed temperature for the device to the sink temperature to which the heat is rejected. We assume that the heat will be rejected to the air and so set the sink temperature equal to the ambient total temperature. Thus when at high altitude, the power required by the cryocoolers is reduced compared to operations on the ground due to the much lower ambient temperature. The power required to remove the heat generated by losses in the cooled devices is assumed to come from the generator and as such is added to the power required from the turbogenerators.

The other cooling method uses liquid hydrogen cooling. Hydrogen has a boiling point of 23 K at 2 atm. Boiling hydrogen is therefore capable of cooling superconductors constructed from MgB2 with an adequate delta T to drive heat transfer. Once the hydrogen has been used as a coolant, it is introduced into the turbogenerator and combusted to provide part of the fuel energy required. The hydrogen mass flow rate required for cooling only represents a small portion of the total energy release necessary. Standard jet fuel is used to provide the remaining fuel energy.

Both cooling methods are compatible with either superconducting material. However, to limit the scope of this study, cryocoolers were only evaluated with BSCCO, and hydrogen cooling with MgB2. The cryocoolers are assumed to all draw power from the common bus in parallel with the fan motors.

All liquid hydrogen properties were obtained from NIST.[15] For liquid hydrogen cooling the following assumptions were made. First all heat removal in the motor and generator stators is assumed to be done by the 451.9 J/g latent heat capacity of the liquid hydrogen. The liquid hydrogen mass flow rate is varied at all operating conditions as required to remove the stator losses entirely with latent heat. The exit temperature of the evolved hydrogen gas from the stators is still at 23 K. In the case of fan motors, the sensible heat capacity of the hydrogen gas coming from the motor is used to remove as much heat as possible from the inverters. If the heat from losses in the inverters is larger than can be removed by hydrogen gas coming from the motor, additional liquid hydrogen is used such that the latent and sensible heat capacity combined of this additional hydrogen will absorb the remaining heat. The heat capacity of hydrogen at temperatures between boiling and about 80 K varies strongly with both temperature and pressure. The average specific heat at 2 atm over the range from boiling to 100 K is 11 J/(kg K).

Table 4. Electrical and Cooling System Design Parameters

Component/Attribute	Parameter	Design Value/Assumptions
Motor/Generator	Efficiency	0.9999
	Tmax (BSCCO)	50K
	Tmax (MgB2)	30K
Inverters	Efficiency	0.9993
	Fraction of losses cooled	0.917
	Tmax	100 K
Cryocoolers	Efficiency (as fraction of Carnot)	0.30
	Tsink	Ambient Total Temperature

III Analysis and Results

A. Fan Design Pressure Ratio Parametric Analysis

The TeDP system described above was run at the ADP to the required net thrust for a range of fan design pressure ratios from 1.15 to 1.5. The residual thrust of the turbogenerators is included in the net thrust. The turbogenerator thrust can change due to changes in airflow required to produce the power required by the fan. As a result only the total thrust of both the turbogenerators and propulsors was constant. The fan efficiency was obtained from Fig. 5 for each design pressure ratio with a 1% penalty applied to reflect the increased fan-face pressure distortion resulting from an embedded installation. The maximum corrected tip speed was obtained from Fig. 6 for each pressure ratio and was used without modification to determine the diameter of the fan. Part of the convergence process was to also determine the number of propulsors that will fit in the 720 inch span with at least a minimum of 4 inch space between. At convergence the number of propulsors with the converged diameter resulted in a total airflow through all of the propulsors that yielded the necessary thrust. Table 5 gives for each design FPR the converged number of propulsors, the fan diameter and the spacing between each fan.

It was assumed that at the design point the height of the stream tube entering the propulsor inlet is the same as the inlet throat height. The inlet height (Inlet area divided by the 720 inch span) is calculated for each iteration of the simulation. As the inlet height varies during the convergence process, the average total pressure and Mach number are recalculated for the new height. Thus when the simulation is converged, the inlet total pressure and Mach number values are those that correspond to the converged value of inlet height. Figure 7 shows the final converged inlet height, and Fig. 8 shows the converged PtRatio and MNratio for each design FPR.

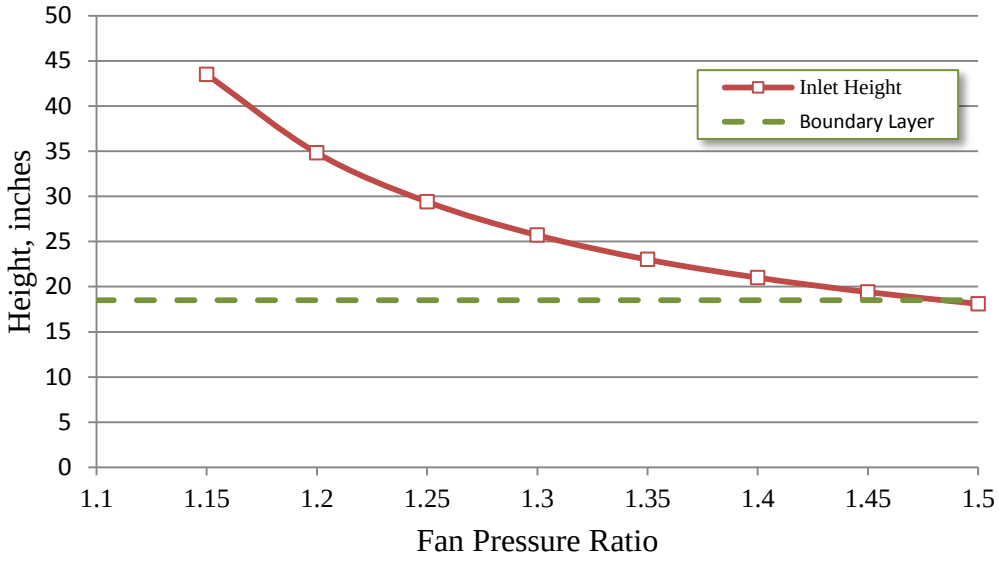

Figure 7. Inlet Height vs. Design Fan Pressure Ratio

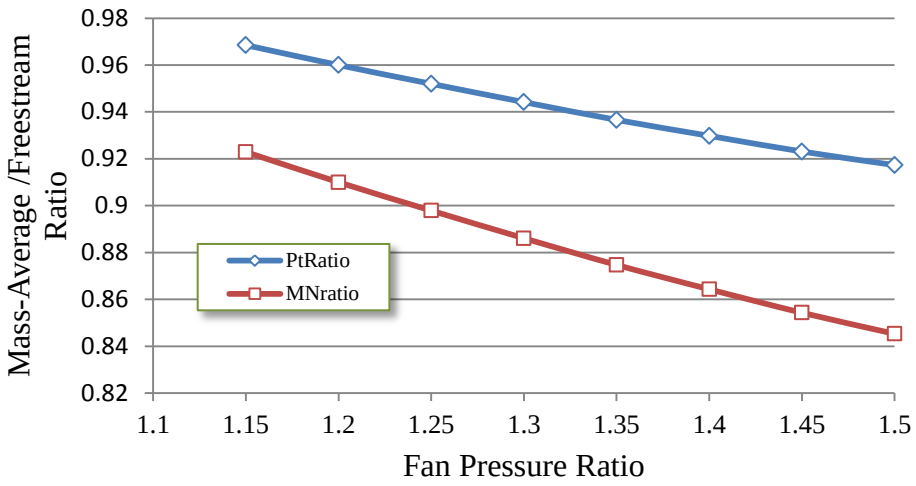

Figure 8. Inlet PtRatio & MNratio vs. Design Fan Pressure Ratio

Equation 1 gives the three terms - freestream velocity, inlet velocity, and nozzle velocity - which determine the propulsive efficiency for embedded inlets. Figure 9 shows how each varies with fan pressure ratio. Included in this figure are the lines for a propulsor of identical design with the inlet MNratio and PtRatio set to 1.0 to represent freestream conditions. The 1% distortion penalty is removed from this freestream propulsor. This minimal change to the existing TeDP model is used rather than constructing a separate turbofan model in order to isolate the effects of changing just the inlet pressure and velocity. Such a system is a fiction since a propulsor could not see freestream conditions without having to be placed on a pylon to lift it well out of the boundary layer. Therefore the results of the freestream propulsor should not be interpreted as being representative of a pylon mounted turbofan.

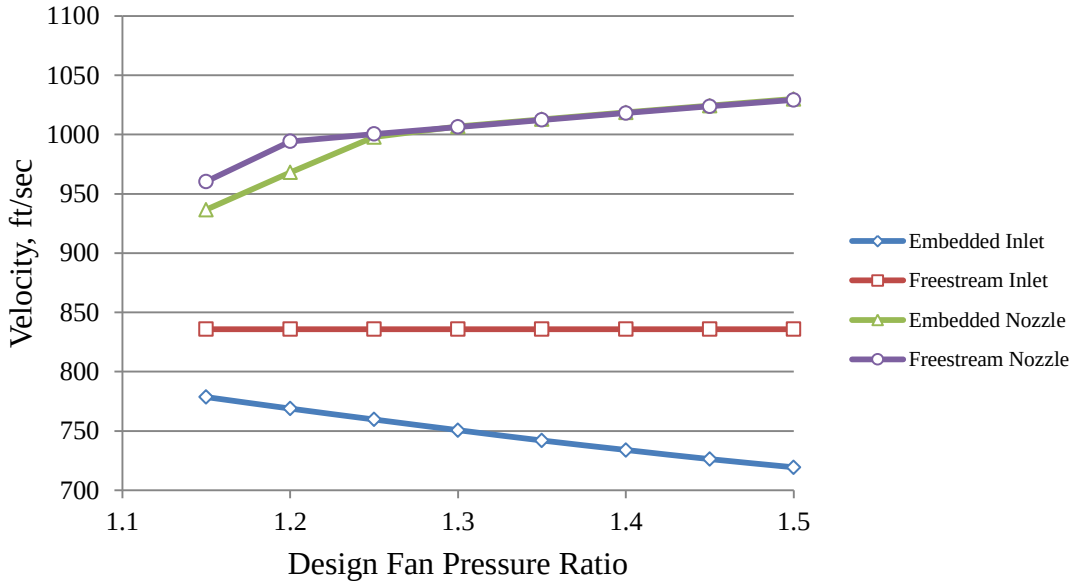

Figure 9. Inlet and Nozzle Velocity for Embedded and Freestream Propulsors

The inlet of the freestream is of course fixed at the freestream velocity for all design fan pressure ratios. For the embedded inlet the situation is different. Increasing the design FPR reduces the mass flow necessary to produce the required amount of thrust. This in turn gives a shorter inlet height. Thus the correlation for embedded propulsors is, the higher the design FPR, the lower the lower the inlet height, and so the lower the inlet velocity. The nozzles of both freestream and embedded propulsors are choked above a fan pressure ratio of 1.25. The reduced inlet pressure of the embedded inlet causes a companion reduction in nozzle pressure ratio. The result is that the embedded nozzle becomes unchoked at a higher pressure ratio than the freestream propulsor. The propulsive efficiency for both the embedded and freestream propulsor are shown in Fig. 10.

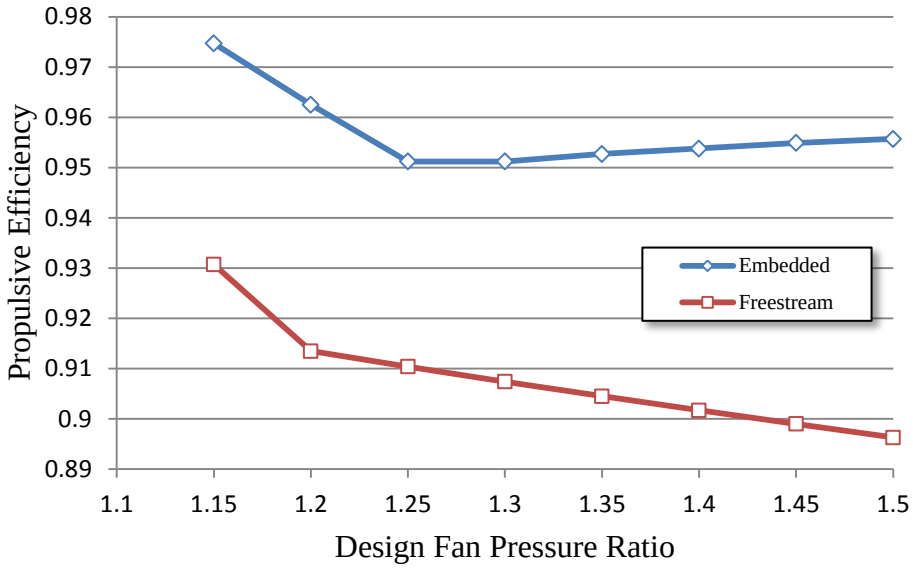

Figure 10. Propulsive Efficiency for Embedded and Freestream Propulsors.

The trend of the freestream propulsor is as expected. The constant inlet velocity and the rapidly increasing nozzle velocity at the lowest design FPR causes the propulsive efficiency to decline rapidly. At a design FPR of 1.20 the nozzle of the freestream propulsor chokes and so the nozzle velocity continues to increase at a slower rate. Yet the inlet velocity is constant, so the propulsive efficiency continues to decline.

The embedded propulsor exhibits two trends. Starting at the lowest fan pressure ratio the embedded propulsor nozzle is unchoked. Adding pressure ratio causes the nozzle velocity to increase more rapidly than the inlet velocity is falling due to the decreasing inlet height, and so the propulsive efficiency decreases. At a fan design pressure ratio higher than 1.25, the nozzle of the embedded propulsor is choked. After this point the nozzle velocity is still rising, but at a rate that is less than the rate at which the inlet velocity is decreasing, and so the propulsor nozzle chokes, the propulsive efficiency begins to increase with increasing fan design pressure ratio.

This counterintuitive result is due to reassessing the inlet average total pressure and Mach number at every design fan pressure ratio. If a single "reasonable" total pressure and Mach number are used, then this result would be missed. Figure 11 shows the difference in propulsive efficiency if a line is added to Fig. 10 for an embedded propulsor where the Pt and MN are held constant. If the inlet conditions at a 25 in high inlet, which corresponds to a design FPR of 1.3, are selected as the values to hold fixed, then Fig. 4 yields values of 0.9426 for PtRatio and 0.8837 for MNratio. At the ADP of 30,000 ft and 0.84 MN the freestream value of Pt is 6.93. This yields inlet conditions of 6.5315 psia and 0.7423 MN.

The figure shows that using the values for PtRatio and MNratio for the range of design FPRs results in a propulsive efficiency with the same general shape as propulsor with freestream value of Pt and MN. However, using single values for Pt and MN overestimates propulsive efficiency by 3% for a design FPR of 1.15 and a underestimates it by 1.7% at design FPR of 1.5.

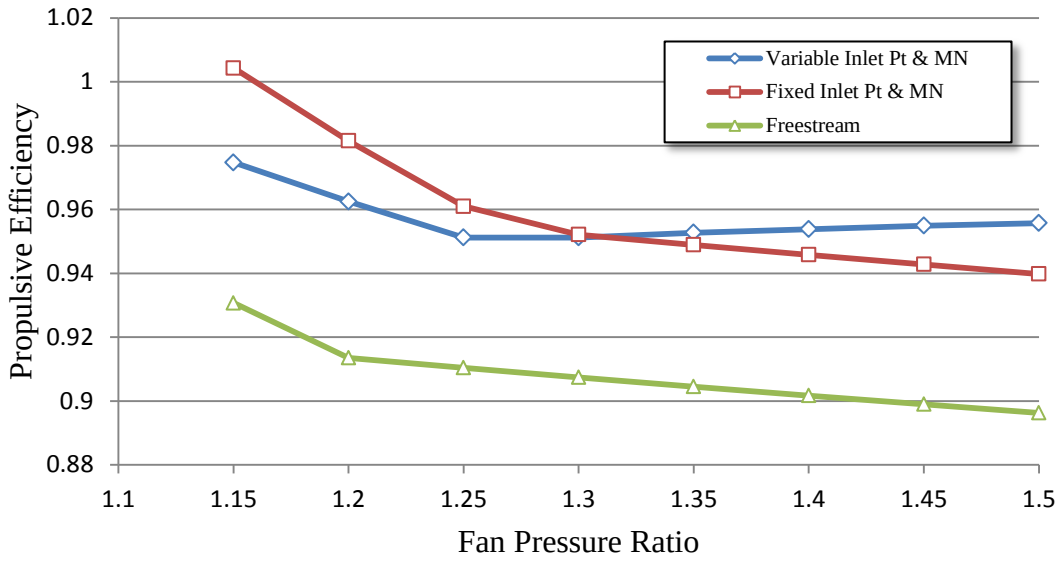

Figure 11. Propulsive Efficiency for Embedded Propulsors with Fixed and Variable Inlet Conditions.

Figure 12 shows the relationship of the installed TSFC of an embedded propulsor with the MN_{avg} and Pt_{avg} recalculated for each design FPR and same propulsion system with freestream propulsor inlet conditions shows the impact of ingesting the boundary layer. The improvement in TSFC ranges from 13% at an FPR of 1.5 to 18% at an FPR of 1.15. As Fig. 12 shows, when the boundary layer computed from the 3-D geometry is used the installed TSFC does not reach a minimum for the design FPRs examined.

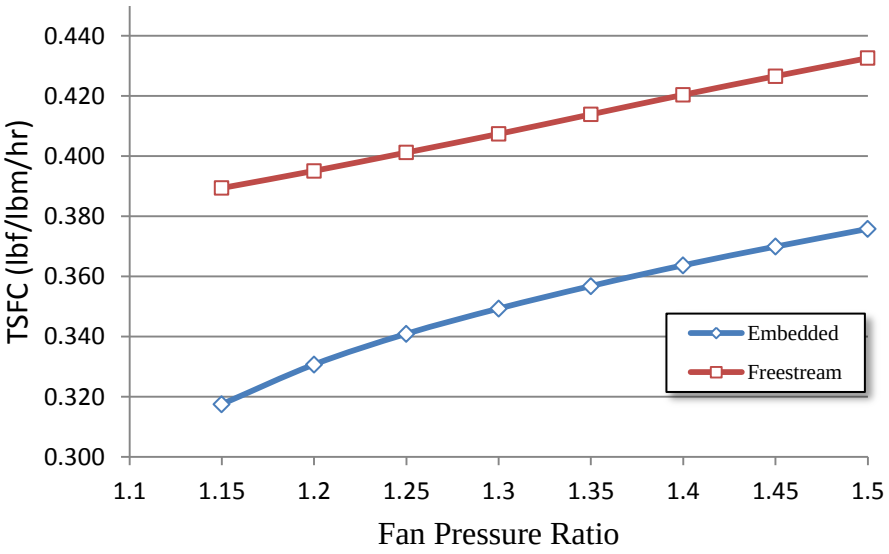

Figure 12. TSFC for Embedded and Freestream Propulsors

Table 5. Design Fan Pressure Ratio Parametric Results

Design Fan Pressure Ratio	1.15	1.2	1.25	1.3	1.35	1.4	1.45	1.5
PtRatio	0.9685	0.96	0.952	0.9442	0.9366	0.9298	0.9231	0.9173
MNratio	0.9229	0.91	0.8979	0.8861	0.8747	0.8643	0.8543	0.8453
Number of Propulsors	9	11	13	15	17	17	19	21
Space Between Propulsors, inches	7.8	7.2	6.2	5.3	4.5	6.3	5.2	4.3
Inlet Width, inches	80	65.5	55.4	48	42.4	42.4	37.9	34.3
Inlet Height, inches	43.5	34.8	29.4	25.7	23	21	19.4	18.1
Fan Efficiency	0.9563	0.952	0.9477	0.9435	0.9387	0.934	0.93	0.926
Fan Diameter, inches	72.2	58.3	49.2	42.7	37.8	36.0	32.7	29.9
Fan Tip Speed, ft/sec	579	680	781	883	989	1095	1198	1300
Fan Shaft Speed, rpm	1748	2544	3467	4512	5701	6630	7997	9471

B. Thermodynamic Cycle Results

A design fan pressure ratio of 1.30 was selected to explore the off-design performance of the TeDP system. Two different configurations, the first using cryocooler refrigeration and the second using liquid hydrogen to maintain the superconductors and power electronics at the necessary cryogenic temperatures were examined. A summary of the off-design performance for the overall system and each of the major subsystems is given at 4 key flight conditions in Tables 6-9.

One key result to highlight is the relatively insignificant amounts of power required to drive the cryocoolers. This is despite the fact that in the cyrocooled cycle the ratio between cooled losses and cryocooler power is 8:1. Even with cryocooler drive power added to the losses in the electrical machinery, the effective transmission efficiency, as measured by the total shaft horse power out of the motors divided by the total shaft horse power into the generators, is greater than 99%.

By eliminating the cryocoolers and the power they draw, the transmission efficiency of hydrogen cooled system jumps to 99.9%. Hydrogen has a second benefit to the system because of its larger lower heating value of 51591 BTU/lbm compared to 18580 BTU/lbm for JetA. The result is that a hydrogen coolant flow rate that represents only 1.7% of the total fuel mass flow results in a 3.6% reduction in TSFC compared to an all JetA fueled system.

Table 6. System Level Performance with Cryocooler and Liquid Hydrogen Cooling

	Cryocooler					Liquid Hydrogen			
System Performance	**Take-off**	**RTO**	**ADP**	**Cruise**		**Take-off**	**RTO**	**ADP**	**Cruise**
alt	0	0	30000	40000		0	0	30000	40000
MN	0	0.25	0.84	0.84		0	0.25	0.84	0.84
dTs	0	27	0	0		0	27	0	0
Fn	124074	67761	26750	16656		124311	67752	26755	16650
WfuelHour	20080	16875	9697	5830		19400	16254	9346	5616
TSFC	0.1618	0.249	0.3625	0.35		0.1561	0.2399	0.3493	0.3373
Wair (Propulsor) (lbm/sec)	5745	5368	2788	1785		5755	5373	2791	1787
Wair (Turbogenerator) (lbm/sec)	198.9	174.1	103.6	66.5		197.2	172.3	102.7	65.9
BPR	28.9	30.8	26.9	26.9		29.2	31.2	27.2	27.1
OPR	69.9	58.1	74.8	75		69.9	58	74.8	75
T3	1798	1810	1681	1603		1798	1809	1681	1602
T4	3460	3412	3260	3110		3460	3410	3260	3110

Table 7. Electrical System Performance with Cryocooler and Liquid Hydrogen Cooling

	Cryocooler				Liquid Hydrogen			
Electrical System	**Take-off**	**RTO**	**ADP**	**Cruise**	**Take-off**	**RTO**	**ADP**	**Cruise**
Total Electrical Power (MW)	54.62	45.68	27.51	16.69	54.50	45.44	27.42	16.63
Generator Electrical Power (MW)	27.31	22.84	13.76	8.35	27.25	22.72	13.71	8.31
Generator Shaft Power (SHP)	36683	30683	18474	11209	36546	30470	18386	11151
Motor Electrical Power (MW)	3.641	3.045	1.834	1.113	3.633	3.029	1.828	0.915
Motor Shaft Power (SHP)	4853	4057	2446	1485	4869	4059	2449	1486
Motor/Generator Losses (KW)	10.92	9.13	5.49	3.34	10.90	9.08	5.48	3.32
Inverter Losses (KW)	36.43	30.47	18.25	11.13	36.35	30.31	18.28	11.09
Cryocooler Power (KW)	382.9	338.5	167.1	94.0	0.0	0.0	0.0	0.0
Parasitic Power (KW)	430.2	378.1	190.8	108.5	47.2	39.4	23.8	14.4
Transmission efficiency	0.9921	0.9917	0.9931	0.9935	0.9991	0.9991	0.9991	0.9991
Whydrogen (lbm/hr)	0.0	0.0	0.0	0.0	327.4	273.0	164.6	99.9
WjetFuel (lbm/hr)	20080	16875	9696	5830	19400	16254	9346	5616

Table 8. Turbogenerator Performance with Cryocooler and Liquid Hydrogen Cooling

	Cryocooler				Liquid Hydrogen			
Turbogenerator	**Take-off**	**RTO**	**ADP**	**Cruise**	**Take-off**	**RTO**	**ADP**	**Cruise**
Wair (lbm/sec)	99.5	87.1	51.8	33.3	98.6	86.2	51.4	33.0
CompL PR	15.62	13.57	16.44	16.49	15.63	13.55	16.44	16.49
CompL efficiency	0.9078	0.9099	0.903	0.9029	0.9077	0.9099	0.903	0.9029
CompH PR	4.47	4.28	4.55	4.55	4.47	4.28	4.55	4.55
CompH efficiency	0.9173	0.9147	0.9184	0.9184	0.9173	0.9146	0.9184	0.9184
TurbH PR	2.2	2.2	2.2	2.2	2.19	2.19	2.19	2.2
TurbH efficiency	0.9502	0.9506	0.9499	0.9496	0.9502	0.9507	0.95	0.9497
TurbL PR	2.6	2.6	2.61	2.61	2.6	2.6	2.6	2.6
TurbL efficiency	0.9426	0.9429	0.9424	0.9421	0.9426	0.9429	0.9424	0.9421
TurbP PR	8.4	7.77	9.55	9.6	8.44	7.8	9.59	9.64
TurbP efficiency	0.9479	0.9486	0.9427	0.9425	0.9476	0.9484	0.9424	0.9422
Nozzle PR	1.343	1.26	2	1.992	1.343	1.259	2	1.992
Nozzle V (ft/sec)	1191	1058	1614	1568	1193	1058	1616	1570
Nozzle MN	0.676	0.596	1	1	0.676	0.595	1	1

Table 9. Propulsor Array Performance with Cryocooler and Liquid Hydrogen Cooling

	Cryocooler					Liquid Hydrogen			
Propulsor Array	**Take-off**	**RTO**	**ADP**	**Cruise**		**Take-off**	**RTO**	**ADP**	**Cruise**
Number of Propulsors	15	15	15	15		15	15	15	15
Wair (lbm/sec)	383	358	186	119		384	358	186	119
Ptamb (psia)	14.696	15.349	6.9292	4.3189		14.696	15.349	6.9292	4.3189
PtRatio	1.000	0.976	0.944	0.944		1.000	0.976	0.944	0.944
MNratio	1	0.9343	0.886	0.886		1	0.9344	0.8861	0.8861
PtCapture (psia)	14.70	14.98	6.54	4.08		14.70	14.98	6.54	4.08
MNcapture	0.000	0.234	0.744	0.744		0.000	0.234	0.744	0.744
Vamb (ft/sec)	0	286.3	835.8	813.5		0	286.3	835.8	813.5
Vcapture (ft/sec)	0	267.7	750.6	730.6		0	267.7	750.7	730.7
Vnozzle (ft/sec)	652.5	647.9	1006.8	980		653	647.7	1006.8	980
Propulsive efficiency	0.000	0.625	0.951	0.951		0.000	0.625	0.951	0.951
Inlet height (in)	25.7	25.7	25.7	25.7		25.7	25.7	25.7	25.7
inletWidth (in)	48	48	48	48		48	48	48	48
Fan diameter (in)	42.66	42.66	42.66	42.66		42.69	42.69	42.69	42.69
Propulsor spacing (in)	5.3	5.3	5.3	5.3		5.3	5.3	5.3	5.3
Fan PR	1.26	1.22	1.3	1.3		1.26	1.22	1.3	1.3
Fan efficiency	0.960	0.969	0.944	0.943		0.960	0.969	0.944	0.944
Fan face MN	0.592	0.542	0.63	0.63		0.592	0.542	0.63	0.63
Fan shaft speed (rpm)	4485	4352	4514	4395		4485	4348	4512	4391
Fan corrected tip speed (ft/sec)	834.97	784.92	882.94	883.09		835.44	784.75	882.94	882.86
Nozzle MN	0.585	0.565	1	1		0.565	0.585	1	1

The speed of the generators and motors is set by the frequency of the AC current they are producing or consuming. The AC-DC-AC transmission path means that the AC frequencies are independent of each other. Figure 13 is a scatter plot of the fan shaft physical speed and the power turbine physical speeds at many operating conditions across the flight envelope. As can be seen there is not a 1:1 ratio between the power turbine and fan speed, and further there is no fixed speed ratio between the shaft speeds. Thus the electrical system in the TeDP can be viewed as a continuously variable ratio gearbox.

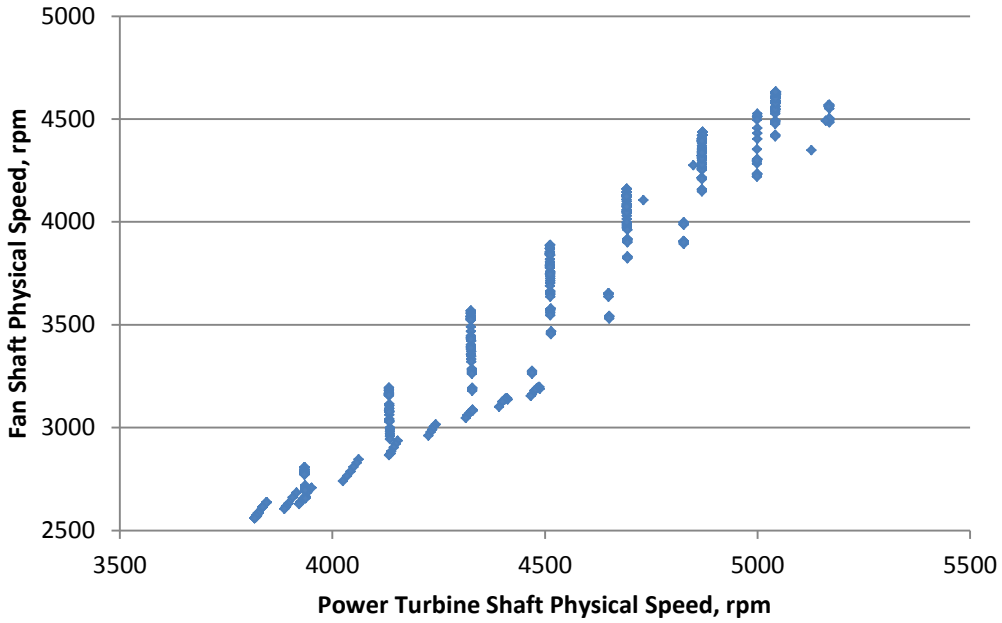

Figure 13. Fan physical speed vs. power turbine physical

The ability to, within limits, control motor and generator speed independently allows the generator and fan motors to change shaft load without changing speed, or change speed without changing the loading. This was used to allow the power turbine and fan to follow a specified operating line. For the power turbine, a corrected speed line of 110% was held constant for all altitudes, speeds and throttle settings. The result is a power turbine that operates within a very narrow range of efficiencies near the peak efficiency of the turbine.

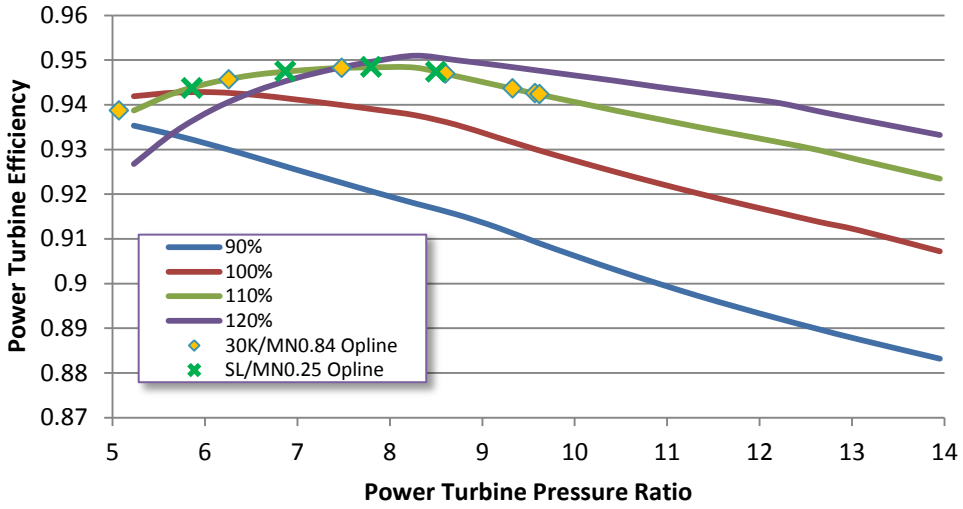

Figure 14. Power Turbine Efficiency vs. Pressure Ratio

For the Fan an R-line of 2.0 was held constant for all altitude, speed and throttle settings. As seen in Fig. 15 the R-line of 2.0 represents the peak efficiency for any corrected speed. By being able to follow this line as the fan can be seen to be running at the highest possible efficiency for a given off-design operating condition.

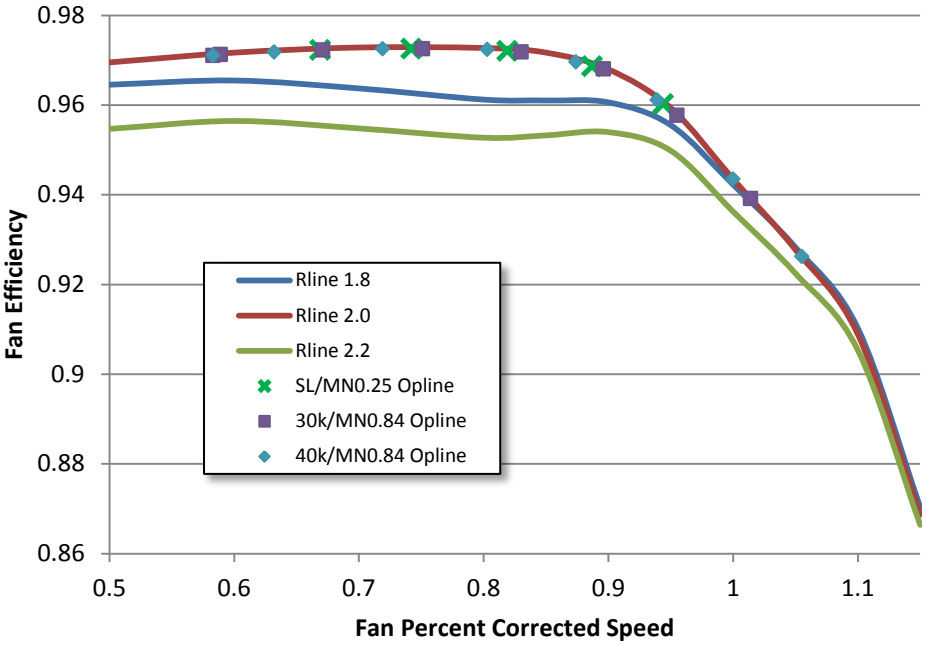

Figure 15. Fan Efficiency vs. Fan Percent Corrected Speed

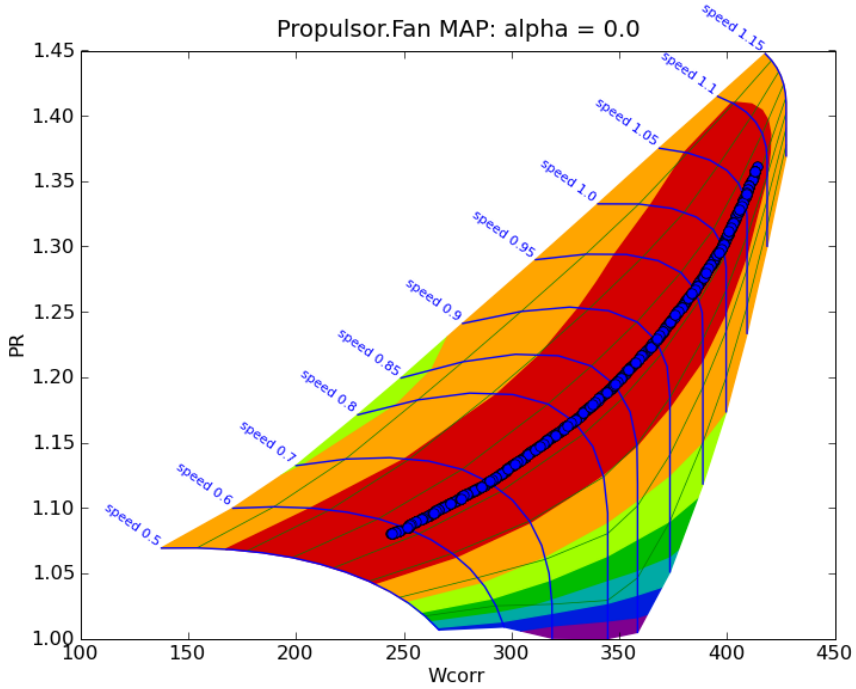

Figure 16. Fan Map with Opline for Full Flight Envelope

C. Effects of Boundary Layer Ingestion on Off-Design Performance

When a pylon mounted engine changes power setting, the amount of air that can pass through the inlet changes as well. As a result the cross sectional area of the freestream tube that contains the air that will pass through the engine changes. If this freestream capture area is smaller than the inlet capture area (defined as the area at the location on the inlet lip that divides air that enters the engine from that spilling around it) then external diffusion occurs. And if the freestream capture area is larger, then there is external acceleration from freestream to the inlet, with subsequent deceleration inside the physical inlet. What does not change is the Pt and MN of the flow in this tube, which remain constant at the freestream values.

The same process occurs with an embedded inlet. However, instead of a freestream capture tube, a capture sheet or stream is a more apt description for the flow field upstream of an embedded inlet, especially in the TeDP system on the N3-X where the aspect ratio is 28:1 for the propulsor array as a whole. With the large total inlet aspect ratio, the span-wise changes in the width of the upstream capture sheet as the propulsor airflow changes would be minor. Thus the key dimension that changes in the capture sheet as propulsor airflow changes is the height. The presence of the boundary layer in the capture sheet, however, means that an embedded inlet will respond very differently to changes in inlet airflow than a pylon mounted engine.

With a pylon mounted engine the total pressure and Mach number of the flow in the freestream capture tube is the same regardless of the diameter of the tube. This is not the case with an embedded inlet. As the height of the capture sheet changes so too does the percentage of the total flow represented by the boundary layer. And in fact the capture height can be shorter than the boundary layer with the top of the boundary layer spilling over the top of the propulsor nacelle. Figure 17 shows the capture sheet height as a function of total net thrust for the ADP. Below a net thrust of about 7,500 lbs, the capture height is less than the boundary layer, and so all of the flow entering the inlet is boundary layer air.

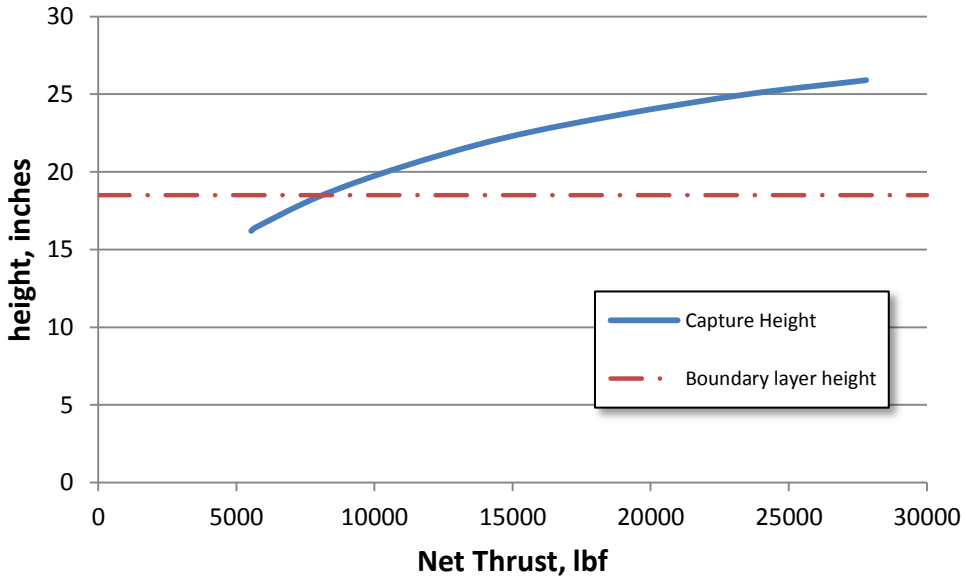

Figure 17. Capture Sheet Height as a Function of Net Thrust at the ADP (30k/MN0.84/ISA)

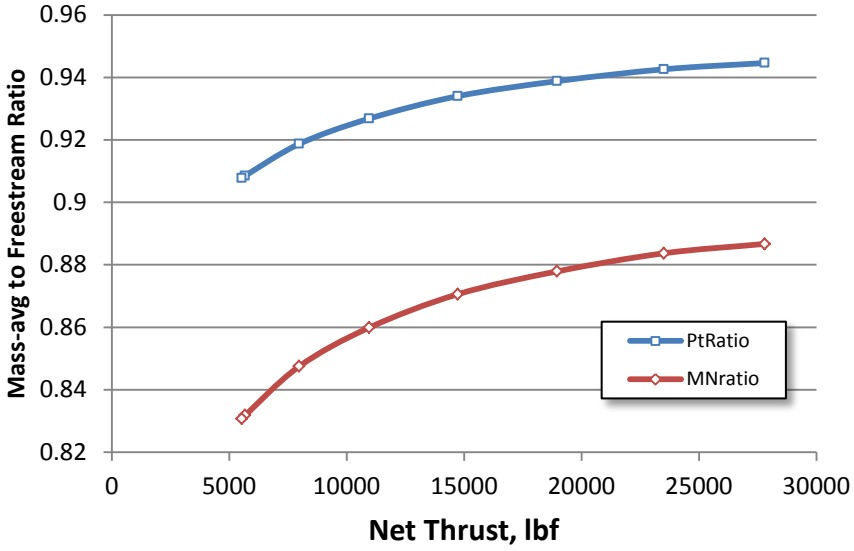

Figure 18. PtRatio and MNratio as a Function of Net Thrust at the ADP (30k/MN0.84/ISA)

The result is that velocity into the inlet is much lower at part power than it is at full power. Thus the propulsive efficiency is also considerably improved. This has a significant effect on the way the propulsion system throttles. The net result is that the Thrust Specific Fuel Consumption (TSFC) vs. Thrust does not exhibit the expected "bucket" where a minimum TSFC is reached at some intermediate thrust level and is higher for both maximum and minimum thrust. As can be seen in Fig. 19, the system instead reaches the minimum TSFC for each flight condition at idle thrust. In fact, the effect of an increasing percentage of the flow being boundary layer air as thrust decreases is so strong that the slope of the curve actually increasing rather than decreasing as thrust approaches idle.

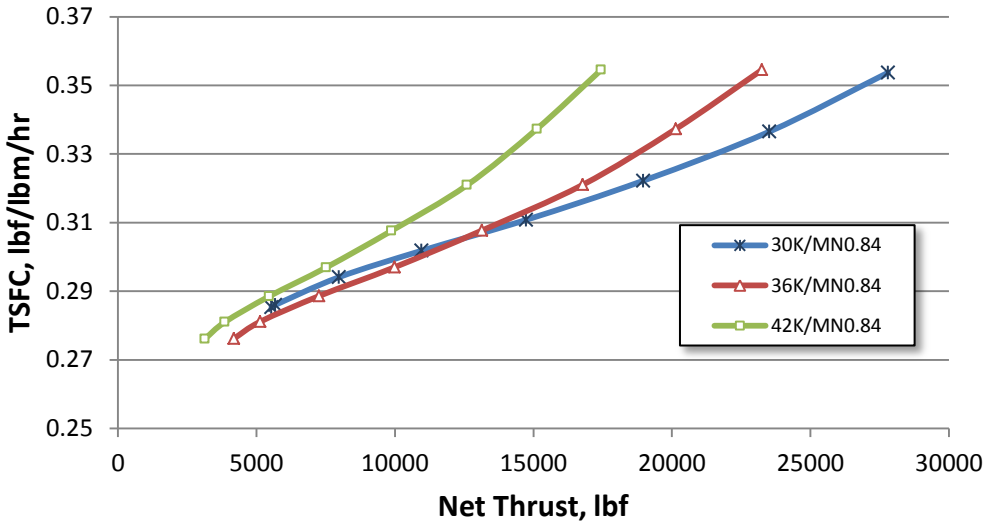

Figure 19. TSFC vs. Net Thrust at the ADP (30k/MN0.84/ISA)

IV Discussion

The fact that changes in design FPR and the resulting increases in fan total area for a given thrust level can be accommodated with minor changes in propulsor array height and with effectively no changes in external wetted area means that design trends of a TeDP system are much different than for podded propulsion system or even embedded system with individual inlets. When examining the off-design characteristics of the TeDP system the changes in propulsor airflow cause the total pressure and Mach number seen by propulsor to fall as the airflow is reduced. The result is that the improvement in propulsive efficiency due lower inlet velocity more than off-set the reduced turbogenerator and fan component efficiencies that in other system cause the TSFC to begin to increase after some partial thrust value where TSFC is a minimum. The net result is that TSFC continues to improve at all partial thrust levels down to idle. This opens up opportunities to explore variations in the design that enhance TSFC at higher power that would not normally be considered do the negative impacts on TSFC at low power.

The improvements in TSFC at very low thrust levels should help to reduce the amount of fuel consumed during the last stages of cruise and during descent, especially for very long range aircraft with high lift to drag ratios such as the N3-X. At the end of cruise the aircraft will be substantially lighter and so will require much less thrust than what was required at the beginning for cruise. Also the high lift to drag ratio means that for a given minimum thrust value the aircraft will have a shallower initial descent and so may spend a longer period of time descending than current aircraft.

A system that doesn't have a TSFC bucket could be ideal for applications like surveillance aircraft which need to minimize fuel burn at the low thrust level during loiter to maximize on station time, while retaining high thrust capacity for short take-off, rapid climb rates and rapid transit speeds. Also of advantage to surveillance and combat aircraft is ability to tap the excess generating capacity in the turbogenerator when flying at a low thrust condition. For example the N3-X flying at 20,000 ft, MN 0.5 requires about 15,800 lbf of thrust which requires about 13.5 MW from the turbogenerators. This is only about 45% of generating capacity of the turbogenerators operating at a max continuous rating at this altitude and speed. At max climb power the turbogenerators capable of generating approximately 30 MW. That means that 16.5 MW is available for tasks other than propelling the aircraft without any extra equipment on the aircraft beyond what is necessary for operation in other flight regimes.

V Conclusion

With an embedded propulsion system, there is no such thing as uninstalled performance. Even the design process must be done with the engine operating installed in the aircraft boundary layer flow field. The quality of the answers obtained therefore is only as good as the quality of the installation effects included. Of prime importance are the details of the boundary layer total pressure and Mach number profiles. Ideally a boundary layer profile is available at the inlet for each individual propulsor inlet in order to capture the span-wise and chord-wise variations in the inlet locations across the width of the propulsor array. In addition the variations in the boundary layer profiles for changes in altitude, Mach number and angle of attach should also be assessed. This analysis should be repeated when this fuller representation of the boundary layer is known.

A simple thermodynamic cycle analysis with limited amount of detailed boundary layer profile information did yield some important insights into how a continuous array of electrically driven propulsors interacts with the boundary layer both during design parametric studies and during off-design analysis of a given design. This analysis, however, did not yield a clear choice in design fan pressure ratio. The 43.5 inch inlet height necessary for even the 1.15 fan pressure ratio is not unreasonable. The fuel burn for the given design thrust continues to decline for all design FPRs examined. The normal countervailing trend of increased nacelle drag due to increases in external wetted area with decreasing FPR is not present in the TeDP system when integrated into a hybrid wing body aircraft. So there is no additional nacelle drag to cause a point of diminishing returns to be reached. Also the vertical variations in the thrust centerline changes only 42 inches from 1.15 to 1.5 design FPR, so changes in pitching moment due to changes in the vertical center of thrust is also not a significant factor in selecting a design FPR.

The results of this analysis indicate that a fan with a pressure ratio as low as will operate behind a boundary layer ingesting embedded inlet should be the one selected. Detailed analysis of the inlet and fan for at least design FPRs of 1.2 and 1.3 should be performed to determine if fans with these pressure ratios are viable in an embedded application such as this. And if they are viable, what is the efficiency that can be achieved.

The compressor performance maps used in the TeDP model in NPSS were not specifically designed with this application in mind. The result is that operation far from the design conditions may have substantial difference from the results obtained using components specifically designed for this application. Therefore the exact thrust and TSFC levels at and near idle should not have too much significance assigned to their absolute numbers. However, we think it

is likely that the effects from increasing the percentage of the inlet flow that is boundary layer flow as the engine throttles down to idle that results in a minimum TSFC at idle is an actual phenomenon that will still be present in a more refined system model.

Acknowledgments

The authors would like to thank Mr. Jeff Berton at NASA Glenn Research Center who provided helpful discussions and insights for this analysis. In addition, special thanks go to NASA's Subsonic Fixed Wing Project principal investigator, Ruben Delrosario, and project scientist, Richard Wahls, for their support on the TeDP research activity.

References

.

[1] Wahls, R., "N+3 Technologies and Concepts", Green Aviation Summit, NASA Ames Research Center, September 8-9, 2010, http://www.aeronautics.nasa.gov/pdf/wahls_2_green_aviation_summit.pdf [cited December 17, 2010]

[2] James L. Felder, Hyun Dae Kim, and Gerald Brown, "Turboelectric Distributed Propulsion Engine Cycle Analysis for Hybrid Wing-body Aircraft", AIAA-2009-1132, presented at 47th AIAA Aerospace Sciences meeting in Orlando, FL, Jan 7, 2009.

[3] Lytle, J.K.: The Numerical Propulsion System Simulation: An Overview. NASA TM-2000-209915

[4] NPSS User Guide Software Release: NPSS_1.6.5

[5] Kawai, Ron, et al, "Acoustic Prediction Methodology and Test Validation for an Efficient Low-Noise Hybrid Wing Body Subsonic Transport", NASA Contract Number NNL07AA54C, 2008.

[8] Plas, A. P., Sargeant, M. A., Madani, V., Crichton, D., Greitzer, E. M., Hynes, T. P., and Hall, C. A., *Performance of a Boundary Layer Ingesting (BLI) Propulsion System.* AIAA paper AIAA 2007-450, AIAA 45th Aerospace Sciences Meeting, January 2007.

[9] Friedman, D., "Aerodynamic Prediction Methodology and Test Validation for an Efficient Low-Noise Hybrid Wing Body Subsonic Transport". NASA Contract NNL07AA54C, 2nd Annual Review, NASA Ames Research Center, January 20, 2010

[10] ICAO Committee on Aviation Environmental Protection: Environmental Design Space (EDS) Prototype. CAEP/7 WG2 -Aircraft Operations and Modeling, TG2 Meeting -Sixth Meeting, Tucson, AZ, 7-8 February 2006

[11] Guyn, M. D., et. al., "Engine Concept Study for an Advance Single-Aisle Transport", NASA TM-2009-215784

[12] Tillman, T.G., "System Study and Distortion-Tolerant Fan Design for a boundary Layer Ingesting Propulsion System", NASA NRA NNC07CB59C Phase 2 Final Report, July 22, 2010

[13] Brown, Gerald V., "Weights and Efficiencies of Electric Components of a Turboelectric Aircraft Propulsion System", 49th AIAA Aerospace Science Meeting, Orlando, Fl, Jan 4th, 2011 (submitted for publication)

[14] "Lightweight, Efficient Power Converters for Advanced Turboelectric Aircraft Propulsion Systems", Final Report, NASA 2010 Phase 1 SBIR, NNX10CC71P, MTECH Laboratories, LLC, July 29, 2010.

[15] E.W. Lemmon, M.O. McLinden and D.G. Friend, "Thermophysical Properties of Fluid Systems" in NIST Chemistry WebBook, NIST Standard Reference Database Number 69, Eds. P.J. Linstrom and W.G. Mallard, National Institute of Standards and Technology, Gaithersburg MD, 20899, http://webbook.nist.gov, (retrieved November 22, 2010)